JAAS

Cite this: *J. Anal. At. Spectrom.*, 2012, **27**, 1667

www.rsc.org/jaas

PAPER

Quantitative Zn speciation in zinc-containing steelmaking wastes by X-ray absorption spectroscopy†

Lihua Wang,[a] Xiaoming Lu,[b] Xiangjun Wei,[a] Zheng Jiang,[a] Songqi Gu,[a] Qian Gao[a] and Yuying Huang*[a]

Received 15th March 2012, Accepted 16th July 2012
DOI: 10.1039/c2ja30094j

To prevent improper handling of zinc-containing steelmaking wastes and find better solutions for recycling these materials, synchrotron induced X-ray absorption spectroscopy (XAS) was used to determine the chemical form of zinc quantitatively at the atomic scale. Five types of zinc-containing steelmaking wastes generated during the production of carbon steel in blast furnace, basic oxygen furnace and blast furnace were collected. In dust collected from the gas-cleaning system of electric arc furnace (EAFD) and basic oxygen furnace developed by Lurgi and Thyssen companies (BOF LT), zinc existed predominantly as franklinite phase ($ZnFe_2O_4$). The presence of Zn–O, Zn–Fe, Zn–Zn bonds in the nearest two coordination shells were observed. In off gas sludge generated in basic oxygen furnace (BOF OG), three main types of zinc species were identified: $Zn_5(CO_3)_2(OH)_6$, $ZnFe_2O_4$ and $ZnSO_4 \cdot 7H_2O$. Zn–O and Zn–Zn bonds occurred in the nearest two coordination shells. Blast furnace dust (BFD) comprised about 39% soluble phase in the form of $ZnCl_2$ and 61% insoluble phase in the form of $ZnFe_2O_4$. In blast furnace sludge (BFS), $ZnCl_2$ was also obtained as the soluble phase and the insoluble phase was zinc silicate possibly in the form of $ZnSiO_3$. These findings deepened our understanding of zinc speciation contained in zinc-containing steelmaking wastes and provided the fundamental information for better dealing with this kind of metallurgical residues.

1. Introduction

One important type of by-product in the steelmaking industry is dust and sludge collected from the gas-cleaning systems during the steelmaking processes. Every year, a large amount of such kind of metallurgical residues is generated. They often have complex composition and contain several components which have negative effects on not only environment but also steelmaking production. Demands from society and enterprise itself have exerted the pressure to minimize the amount of metallurgical residues and find an appropriate way to treat these wastes and recycle their valuable components.

Zinc is one of those elements which should be paid attention to in particular. This element is easy to volatilize during the metallurgical process due to the boiling point of zinc below the melting temperature in furnace and subsequently condenses and accumulates to form particles in the form of dust or sludge when passing through the gas-cleaning system. Usually this dust and sludge causes risks in two ways. One is the negative influence on the environment. This kind of metallurgical residue is often composed of fine particles, it can be easily discharged into the atmosphere and accumulates in soils during transportation and landfill. Although zinc is an essential element for humans and plants, it can cause zinc poisoning and environmental risks when its concentration becomes high.[1,2] The second is about the negative effect on steelmaking production. Generally dust and sludge must be disposed of at a hazardous waste disposal site, which brings high transport and disposal costs. These costs could be reduced if metals, such as iron, zinc, and so on, could be recovered or sold. The most common way to utilize this dust and sludge is reusing them as a secondary source of raw material due to the high iron content. However, when they are reused inside enterprises, undesirable consequences will occur. In particular, the presence of zinc will damage the production equipment. Take blast furnace for example. When the dust and sludge are back recycled in a blast furnace, zinc will accumulate on the walls, penetrate the lining, take part in the lining's deformation and disintegration and subsequently damage the blast furnace.[3,4]

Since the mobility of inorganic elements largely depend on their chemical forms, it is necessary for us to obtain a thorough knowledge of zinc speciation. Traditionally, the most common method used to obtain zinc speciation in zinc-steelmaking wastes is X-ray diffraction (XRD). However, there are two obstacles when applying XRD in zinc-containing steelmaking wastes. Firstly, XRD is sensitive to phases with good crystallinity. So far

[a]*Shanghai Synchrotron Radiation Facility, Shanghai Institute of Applied Physics, Chinese Academy of Sciences, Shanghai 201204, P. R. China. E-mail: huangyuying@sinap.ac.cn*
[b]*Research Institute, Baoshan Iron and Steel Co., Ltd., Shanghai 201900, P. R. China*

† Electronic supplementary information (ESI) available. See DOI: 10.1039/c2ja30094j

only electric arc furnace dust (EAFD) which has high zinc content has been detected by means of XRD. Zincite (ZnO) and franklinite ($ZnFe_2O_4$) are the two most common phases which have been obtained in EAFD.[5–8] For dust and sludge generated in blast furnace and basic oxygen furnace, which has relatively low Zn content and poor degree of crystallinity, it is difficult to get zinc speciation using XRD method. Secondly, for Fe_3O_4 and $ZnFe_2O_4$, their XRD patterns are very close.[9–11] As a result, it is impossible to determine which phase gives the X-ray pattern or if both phases are present.

In previous years, X-ray absorption spectroscopy (XAS) has proven itself as a powerful technique for structural characterization of the local atomic environment of a certain element, including bond distance, coordination numbers and types of nearest neighboring atoms surrounding the central atom. In particular, this technique is useful for material which has complex composition and poor crystallinity. Up to date, a number of XAS studies have been carried out to get the speciation of toxic metal elements contained in soils and sediments,[12–17] fly ashes,[18–20] atmospheric particulates,[21] tailings,[22–24] and so on.

Based on the above considerations, five types of zinc-containing steelmaking wastes were collected. The basic information in bulk, including chemical composition and mineral phases, was firstly obtained by means of X-ray fluorescence and X-ray diffraction. Then Zn K-edge XAS spectroscopy measurements were carried out to get the zinc speciation at the molecular scale. The purpose of this research was to deepen our understanding of the zinc speciation in these dust and sludge. Consequently better solutions for handing these metallurgical residues could be found and valuable components recycled as much as possible.

2. Samples and methodologies

2.1 Samples

Samples analyzed here include electric arc furnace dust (EAFD), blast furnace dust (BFD) and sludge (BFS), off gas sludge generated in basic oxygen furnace (BOF OG), dust collected from the gas-cleaning system of basic oxygen furnace developed by Lurgi and Thyssen companies (BOF LT). All these samples were collected from the gas-cleaning system generated during the carbon steelmaking processes at a steelmaking plant in China. In this plant, about 800 thousand tons of dust and sludge are generated every year. Among these residues, about 200 thousand tons of zinc-containing dust and sludge are not adequately dealt with.

2.2 Methodologies

2.2.1 X-ray fluorescence. X-ray fluorescence (XRF) was carried out by wavelength dispersive X-ray fluorescence (ARL 9900, Thermo Fisher Scientific, Switzerland). Prior to XRF analysis, each sample was firstly baked at 105 °C for 2 hours and then fired at 1050 °C for 1 hour. After it cooled, each sample (0.7 g), together with lithium tetra borate (7.0 g) and cobalt oxide (0.07 g), was placed in a platinum crucible and melted at 1100 °C in a furnace for 20 minutes to form a glass bead which could be used to detect the content of each element by means of wavelength dispersive X-ray fluorescence. Elements analyzed here include Fe, Zn, Al, Si, Ca, Mg, Mn and P. All the XRF analyses were carried out at voltage 40 kV, and current 60 mA.

2.2.2 Synchrotron radiation X-ray diffraction. Synchrotron radiation X-ray diffraction (SR-XRD) measurements were performed on BL14B beamline at Shanghai Synchrotron Radiation Facility (SSRF), Shanghai, China, with a fixed wavelength of 1.239 Å. Storage ring was operated at the energy of 3.5 GeV with the current from 130 mA to 210 mA. Data collection was done in a continuous 2θ-scan mode with 0.025° step and 1 s acquisition time per point.

2.2.3 XAS experiments and data analysis. Zn K-edge XAS spectra were recorded at BL14W beamline at Shanghai Synchrotron Radiation Facility (SSRF), Shanghai, China. Storage ring was operated at the energy of 3.5 GeV yielding an electron beam of 130–210 mA. A total of 9 reference spectra were considered, including zinc metal foil, $ZnFe_2O_4$, ZnO, ZnS, $ZnSO_4 \cdot 7H_2O$, $Zn_5(CO_3)_2(OH)_6$, $Zn_3(PO_4)_2$, $ZnCl_2$, $ZnSiO_3$. Except zinc metal foil, all other zinc compounds were bought from Sinopharm Chemical Reagent Co., Ltd, a chemical reagent company in China. All Zn reference spectra were collected in transmission mode using ionization chambers. Prior to XAS experiments, each zinc compound was diluted with lithium fluoride to obtain an edge jump of about one. For zinc-containing steelmaking wastes, each sample was ground using an agate mortar and sieved (400 mesh) to ensure the small size of particles. Then powder samples were spread evenly onto a 3M tape and used for the XAS spectra collection. During the experiments, different detectors were used based on the Zn content contained in each sample. For EAFD, XAS spectrum was recorded in transmission mode using ionization chambers. For BFS and BFD, XANES spectra were recorded in fluorescence mode using 4-element silicon drift detector. During the above experiments, Si(311) double crystal monochromator was used and high harmonics were rejected by detuning the monochromator to reduce the intensity of I_0 by 20%. As for BOF OG and BOF LT, Si(111) double crystal monochromator was used and rejection of high harmonics was obtained using harmonics mirror with Rh layer. The XAS spectra were recorded in fluorescence mode using a Stern–Heald-type (Lytle) detector. Depending on Zn and Fe concentrations, several scans were averaged to improve the signal-to-noise ratio of EXAFS spectra.

Data reduction was carried out using the ATHENA program in IFEFFIT package following standard procedures.[25] Background was subtracted by a linear equation that was fitted in the pre-edge region and a polynomial function was used to fit the EXAFS region. By comparing the first derivative spectra of zinc-containing steelmaking wastes with that of reference materials, those reference materials with similar characteristics were selected to do the linear combination fit (LCF) using ATHENA software in order to identify the possible zinc species. The fitting range was from −20 eV to 50 eV with respect to the energy of zinc K-edge. Fitting was optimized by minimizing the residue of the fit. The best fit was obtained when R-factor was minimized. Here R-factor was defined as $\sum(\mu_{exp} - \mu_{model})/\sum\mu_{exp}$ where the sums were over the data points in the fitting region (Table 1).[26]

EXAFS data analysis was processed with the aid of ATHENA and ARTEMIS program in IFEFFIT package.[25] In brief,

Table 1 Results of linear combination fit of the Zn K-edge XANES spectra for zinc-containing steelmaking wastes

	EAFD	BOF LT	BOF OG	BFD	BFS
ZnO (%)	11				
$ZnFe_2O_4$ (%)	89	100	24	61	
$ZnCl_2$ (%)				39	34
$ZnSiO_3$ (%)					66
$Zn_5(CO_3)_2(OH)_6$ (%)			46		
$ZnSO_4 \cdot 7H_2O$ (%)			30		
R (%)[a]	0.08	0.28	0.37	0.09	0.24

[a] Means the R-factor which is defined as $\sum(\mu_{exp} - \mu_{model})/\sum\mu_{exp}$ where the sums are over the data points in the fitting region.

EXAFS oscillations, $\chi(k)$, were extracted from the normalized XAS spectra and transformed over the range 2.5–12 $Å^{-1}$ from k-space to R-space with k^3 using Hanning window to obtain the radial structure function (RSF). Location of the peaks in the RSFs represents the distances between the absorber and the successive neighboring atoms. Contributions of the first and second shell were isolated by inverse Fourier transformation over the appropriate region and fitted based on the single scattering EXAFS equation. Phase-shift and backscattering amplitude functions for structural fitting of EXAFS spectrum were generated using FEFF8.2 from the structures of $ZnFe_2O_4$ and $Zn_5(CO_3)_2(OH)_6$ for Zn–O, Zn–Fe and Zn–Zn scattering paths.[27,28] During the fitting, amplitude reduction factor (S_0^2) was fixed at 0.85 which was calculated with the EXAFS spectrum of ZnO. Residues used to evaluate the quality of fits were the square root of the average square difference between experimental and calculated data.

3. Results

3.1 Results of XRF and SR-XRD

The chemical compositions of zinc-containing steelmaking wastes analyzed here are summarized in Table S1.† All these samples had a high content of iron (from 38.0% to 60.2%). In EAFD, Zn content was 20.4 wt% which agrees well with previous findings that EAFD from carbon steelmaking processes often contain high zinc content.[29,30] For dust and sludge from basic oxygen furnace (BOF LT and BOF OG), Zn content was 1.6 wt% and 3.4 wt%, respectively. The total Zn content of the input charge should not exceed 0.05%,[3] BOF OG and BOF LT should be pretreated or mixed with other materials to reduce the content of zinc before reusing in steel production. The content of zinc in BFD and BFS were 0.06 wt% and 0.03 wt%, respectively. Among these elements analyzed here, Ca should not be neglected due to its relatively high content in EAFD, BOF OG and BOF LT. The high content of Ca might be attributed to the lime added to the steelmaking furnace.[31]

Results of SR-XRD analysis of zinc-containing steelmaking wastes were reported in Fig. S1† and details were summarized in Table S2.† In EAFD, Si occurred as quartz. The phase of magnetite and franklinite were also observed. In dust and sludge from blast furnace (BFD and BFS), the presence of hematite and quartz were clearly detected. In BOF OG, Fe occurred as metallic iron and iron oxide; Ca occurred as calcite. In BOF LT, the presence of metallic iron, iron oxide, hematite and calcite were clearly identified. Magnetite and franklinite might be present. However, just as previous studies point out, the signals from magnetite and franklinite phases exhibited overlapping to some extent.[10,11] Due to its overlapping, it is difficult to distinguish their phases. As a result, the presence of zinc minerals could be hardly detected in such kind of zinc-containing steelmaking wastes only by means of XRD method.

3.2 XAS results

3.2.1 Linear combination fit of XANES spectra. Zn K-edge XANES spectra of five types of zinc-containing steelmaking wastes and nine reference materials are illustrated in Fig. 1(a). To show the XANES features clearly we also show the first derivative of all XANES spectra in Fig. 1(b), where three vertical dotted lines running through derivative curves are used as a guide for the eye. As can be seen in Fig. 1, each compound shows their XANES features clearly. In brief, the XANES spectrum of $ZnFe_2O_4$ shows three resolved peaks at around 9665, 9669, and 9673 eV, respectively, a shoulder at around 9679 eV, and an additional structure at higher energies (~9686 eV). While Zn K-edge XANES spectrum of $ZnSiO_3$ has two resolved peaks at around 9665 and 9669 eV, respectively. The XANES features of ZnO were the white line peak at around 9669 eV, a shoulder at around 9664 eV, and the additional structure at around 9680 eV. For the others, the white line peaks were at around 9669, 9665, 9669, 9668, 9666, and 9665 eV for Zn metal foil, ZnS, $ZnSO_4 \cdot 7H_2O$, $Zn_5(CO_3)_2(OH)_6$, $Zn_3P_2O_8$, $ZnCl_2$, respectively.

From observation, Zn K-edge XANES spectra of EAFD and BOF LT had similar characteristics with that of $ZnFe_2O_4$: three resolved peaks, a shoulder and an additional structure at higher energies (indicated A, B, C, D and E in Fig. 2(a) and (b)). Compared with $ZnFe_2O_4$, intensity of peaks B and D for EAFD

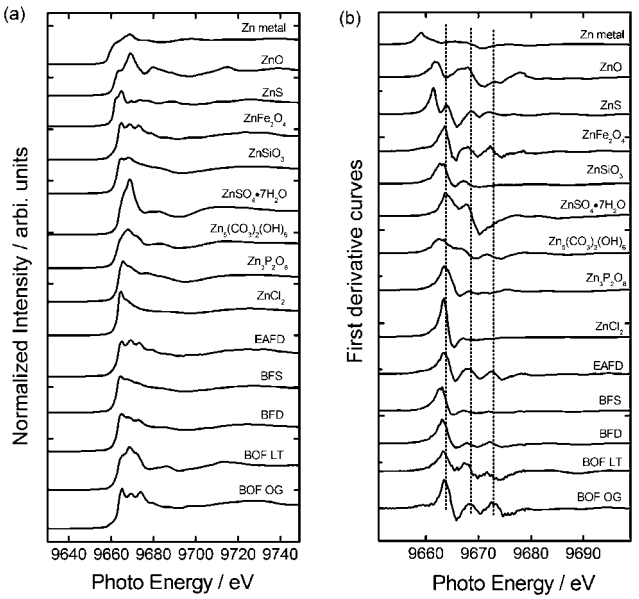

Fig. 1 Comparison between spectra of reference materials and zinc-containing steelmaking waste samples in bulk: (a) experimental data at the Zn K-edge; (b) first derivative of the curves of panel (a).

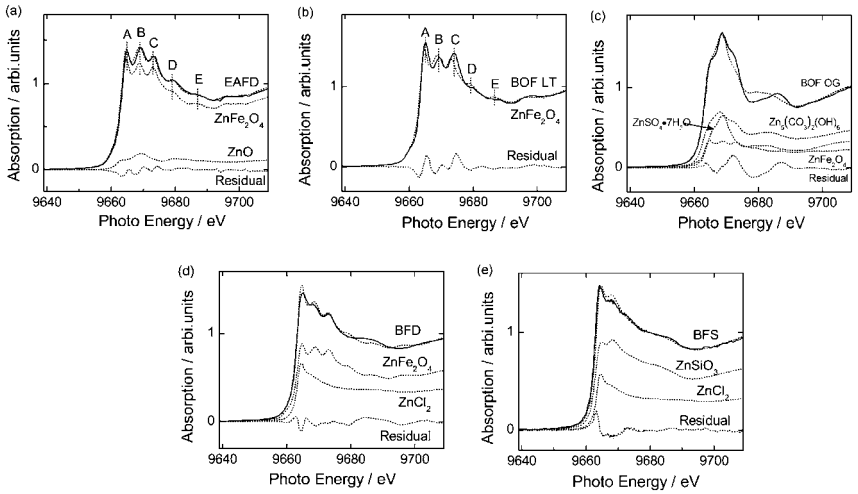

Fig. 2 Results of the linear combination fit (LCF) for the XANES spectra of zinc-containing steelmaking wastes: (a) EAFD; (b) BOF LT; (c) BOF OG; (d) BFD; (e) BFS. The solid line denotes the experimental data and the dotted line indicates the fitting result and reference materials used to do LCF fit. Peaks A, B, C, D and E in panel (a) and (b) referred to the XANES features for $ZnFe_2O_4$, EAFD and BOF LT, including three resolved peaks at around 9665, 9669, and 9673 eV, a shoulder at around 9679 eV, and an additional structure at higher energies (~9686 eV), respectively.

increased. There are two possibilities that might induce the increasing of peak B. One is the important fraction of Zn located at octahedral sites.[32–34] Ideally, Zn usually occupies tetrahedral sites and Fe at octahedral sites in normal spinel $ZnFe_2O_4$. When Zn at octahedral sites is considered due to the high degree of disorder, the intensity of peak B will increase. The other possibility is the presence of zincite (ZnO). Because the white line of zincite (ZnO) is around 9669 eV (peak B) and an additional structure is around 9680 eV (peak D). For the first possibility, intensity of peak D will weaken as the increasing of intensity of peak B, which is not consistent with the XANES features of EAFD. Thus we hypothesized the presence of ZnO in EAFD. Since LCF analysis of XANES spectra in recent years has been successfully employed to identify and quantify the major zinc species in fly ashes,[35,36] the linear combination fit of the above two compounds was performed. The best fitting result shows that calculated data with 89% $ZnFe_2O_4$ and 11% ZnO reproduced the experimental data very well. In the case of BOF LT, its XANES features, both energies and intensity of peak A, B, C, were similar with that of normal spinel $ZnFe_2O_4$ or franklinite, a zinc-bearing spinel phase with an approximate formula (Zn, Fe, Mn)(Fe, Mn)$_2O_4$.[12,37] Thus 100% $ZnFe_2O_4$ was used to fit the experimental data. Other zinc species were tried to be added in order to improve the fitting result. But they did not improve the result well. This finding indicates that zinc was predominantly present as franklinite phase in BOF LT.

Zn K-edge XANES spectrum of BOF OG also showed its particular features. Compared with XANES spectra of these reference materials, it was easy to observe that XANES features of BOF OG were close to that of hydrozincite ($Zn_5(CO_3)_2(OH)_6$). From the comparison of first derivative curves, we identified $Zn_5(CO_3)_2(OH)_6$, $ZnFe_2O_4$, $ZnSO_4 \cdot 7H_2O$ and $ZnCl_2$ as the most likely species. The best fitting result was obtained with the combination with 45% $Zn_5(CO_3)_2(OH)_6$, 30% $ZnSO_4 \cdot 7H_2O$ and 24% $ZnFe_2O_4$. As shown in Fig. 2(c), the calculated data do not agree well with experimental data. The probable reason of the disagreement may be the high degree of inhomogeneity of the sludge particles which may cause local distortions or contain other zinc species which can not be identified here.

For BFD, besides the white line peak at around 9665 eV, two resolved shoulders at around 9668 and 9673 eV were also observed. Zn compounds, including $ZnFe_2O_4$, $ZnCl_2$, $Zn_3P_2O_8$ and $ZnSiO_3$ were considered as the most likely species. The best fitting result showed that $ZnFe_2O_4$ prevailed (61%) in BFD. The other Zn species might present was $ZnCl_2$. In case of BFS, in addition to the white line peak at around 9665 eV, only one shoulder at around 9669 eV could be observed. The best fitting result showed that the main components present in BFS were $ZnCl_2$ and $ZnSiO_3$ with relative fractions of 34% and 66%, respectively. The main difference between experimental and calculated data was the XANES feature at around 9667 eV (Fig. 2(e)). In steel industry, quartz (SiO_2) and zincite (ZnO) can form a series of compounds, such as $ZnO \cdot SiO_2$, $2ZnO \cdot SiO_2$, $ZnO \cdot 2SiO_2$, and so on. Among these compounds, willemite ($2ZnO \cdot SiO_2$), was considered as the most common form.[38] Therefore $2ZnO \cdot SiO_2$ which was not used here as the reference material might be the main reason inducing the disagreement.

3.2.2 EXAFS result. Fig. 3 shows the EXAFS oscillations with k^3 and RSFs with no phase correction for a series of reference materials and three types of zinc-containing steelmaking wastes, including EAFD, BOF LT and BOF OG. As shown in Fig. 3(b), the radial structure function (RSF) of EAFD and BOF LT were similar to that of $ZnFe_2O_4$, which agrees well with the results obtained by the LCF analysis of XANES spectra. The first peak in RSF around $R + \Delta R \sim 1.5$ Å was the result of Zn–O backscattering and the second peak around $R + \Delta R \sim 3.10$ Å might be the contribution of Zn–Fe and/or Zn–Zn backscattering. For BOF OG, the RSF features at around $R + \Delta R \sim 1.55$ Å was the contribution of Zn–O backscattering and the RSF features at around $R + \Delta R \sim 2.68$ Å might be the result of Zn–Zn or Zn–Al backscattering.[39] Thus, for EAFD and BOF LT, fitting was carried out with Zn–O first shell in combination with second shell Zn–Fe and Zn–Zn. For BOF OG, fitting was

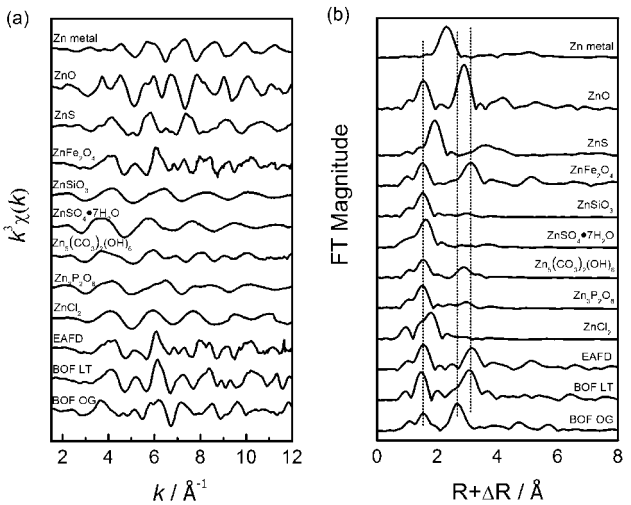

Fig. 3 EXAFS oscillations, $\chi(k)$, with k^3 weight (a) and k^3-weighted, phase uncorrected FT (b) for reference materials and zinc-containing steelmaking wastes.

processed with Zn–O first shell in combination with second shell Zn–Zn. Here Zn–Al bond was ruled out due to the lack of splitting of first oscillation at around 3.8 Å^{-1} which has been attributed to Al atoms in the second coordination shell.[40] The best fitting results are illustrated in Fig. 4 where the experimental data are illustrated with a solid line, and the calculated data with solid circles.

As can be seen in Fig. 4, the calculated data reproduced the experimental data well. Details of structural parameters are summarized in Table 2. For EAFD, the distance of Zn–O bond was about 1.97 Å with coordination number of 4.1 and the distance of Zn–Fe and Zn–Zn were at 3.58 Å and 3.88 Å with coordination numbers of 11 and 6.3, respectively. For BOF LT, Zn was surrounded by 4 O atoms at a distance of 1.98 Å, 13.5 Fe atoms at 3.45 Å, and 8.6 Zn atoms at 3.63 Å. The above fitted structure parameters are in line with that of franklinite.[12] For BOF OG, the best fitting result shows that the distance between

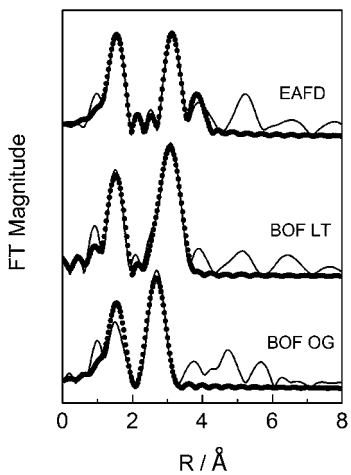

Fig. 4 The best fitting results of the first two shells in RSFs in R space for zinc-containing steelmaking wastes. Experimental and calculated values are illustrated by solid line and solid circles, respectively.

Table 2 Results of fitting EXAFS data for zinc-containing steelmaking wastes. R, CN, σ^2 refer to inter-atomic distance, coordination number and Debye–Waller factor, respectively

Sample	Shells	CN	R (Å)	σ^2 (Å^2)[a]
EAFD	Zn–O	4.1 ± 0.8	1.97 ± 0.01	0.005
	Zn–Fe	11.0 ± 2	3.58 ± 0.02	0.01
	Zn–Zn	6.3 ± 3	3.88 ± 0.05	0.01
BOF LT	Zn–O	4.0 ± 0.8	1.98 ± 0.03	0.005
	Zn–Fe	13.5 ± 3	3.45 ± 0.04	0.01
	Zn–Zn	8.6 ± 3	3.63 ± 0.07	0.01
BOF OG	Zn–O	4.5 ± 1	2.01 ± 0.03	0.007
	Zn–Zn	14.7 ± 3	3.05 ± 0.02	0.016

[a] Parameter was varied in initial fits and then fixed with the best value during the final fit.

Zn and O was 2.01 Å and Zn–Zn distance was located at 3.05 Å. In general, zinc is tetrahedrally coordinated with oxygen atoms at a typical distance of $R = 1.95 \pm 0.03$ Å and distance between Zn and O is approximately from 2.06 to 2.08 Å for octahedral coordination.[10,41–43] The Zn–O distance indicates the mixtures of tetrahedral and octahedral sites where zinc atoms are situated.

4. Discussion

As a valuable source of iron and zinc, zinc-containing steelmaking wastes have attracted considerable attention. At the present time, there are several ways to manage these wastes depending on zinc content. If the zinc content in dust and sludge could be reduced to a low content (*e.g.* <0.4%), it can be directly recycled in the iron-making or steel-making process. For zinc-containing wastes with high zinc content (*e.g.* >10%), hydrometallurgical processes are often used to extract the valuable component, especially zinc element. As for zinc content which is between the above, pyrometallurgical process and/or in combination with appropriate pre-treatments are the best choice to handle these wastes.[44,45]

Since the zinc content in EAFD was about 20 wt%, it was a valuable source of zinc. Results of both XANES and EXAFS analysis showed that $ZnFe_2O_4$ in EAFD took up an important proportion (89%) which is greater than that formerly assumed (50% or less).[46–48] In most cases, zinc is extracted by hydrometallurgical processes in order to recycle such zinc-containing steelmaking wastes. However, $ZnFe_2O_4$ has a spinel structure and is very stable and insoluble in most acidic, alkaline and chelating media under mild conditions.[6,7,45,49] Consequently it causes problems in zinc recovery by hydrometallurgical processes. Sodium hydroxide, which is effective in the dissolution of zinc and without significant dissolution of iron, is considered as a better option of leaching agent to extract the zinc component in $ZnFe_2O_4$.[8,50] Thus XAS results suggested that a process mainly consisting of leaching zinc with sodium hydroxide is a good option to treat EAFD here.

Compared with EAFD, little is known about the zinc speciation in dust and sludge collected from gas-cleaning systems of basic oxygen furnace (BOF). XAS analysis indicates that in BOF LT, zinc was predominantly present in $ZnFe_2O_4$ phase, which was very stable and could be disposed safely in landfill. In China, a common way to recycle BOF LT dust is cold hardening process

followed by adding into materials for sintering. In future, the stability of zinc species should be taken into account during the recycling of BOF LT. On the contrary, in BOF OG, the leachable zinc species, $Zn_5(CO_3)_2(OH)_6$ and $ZnSO_4 \cdot 7H_2O$, accounted for a significant content (~76%). These results suggest that washing process could be arranged firstly to remove the leachable part in order to reduce zinc content in BOF OG. Then several options could be considered for the solid residues, such as back-recycling to the blast furnace, a more safe dumping due to its relatively inertness, and so on.

Generally, zinc content in blast furnace dust and sludge was relatively low (<0.1%) so that it could be reused as a secondary source of iron in blast furnace for iron-making or steel-making production. However, XANES results suggested that $ZnCl_2$ were present in both BFS and BFD, which were also detected in EAFD by wet chemistry in previous research.[51] As previous studies point out, the existence of chlorine element will speed up the evaporation of zinc at high temperatures.[10,35] As a result, when BFD and BFS were reused in blast furnace, zinc was so easy to evaporate that it lead to the enrichment of zinc in the exiting flue gas. Although it was impossible to estimate the influence quantitatively here, the possibility that chlorine would accelerate the mobility of zinc at high temperatures should be taken into account. Therefore, the best way to recycle BFS and BFD is to remove chlorine element first by washing processes and then the solid residues could be reused in blast furnace.

From the present study here, it was clear that XAS has its advantage to obtain chemical form of zinc element in zinc-containing steelmaking wastes. These results could provide us more fundamental information which was very useful for improving the recycling methods. However, results obtained by XAS analysis here were not a conclusive identification because some other possible significant compounds, such as Zn_2SiO_4, were not examined. If these reference materials were incorporated, findings here could be changed subsequently. Therefore, the result presented here is rather a proof-of-principle than a fully quantitative one. In future research, a larger set of reference materials, as well as more samples, will be considered in order to get more conclusive identification.

5. Conclusions

To summarize, results obtained by linear combination fit (LCF) of X-ray absorption near edge structure (XANES) spectra revealed that zinc mainly existed as franklinite phase ($ZnFe_2O_4$) in EAFD and BOF LT. In BFD and BFS, $ZnCl_2$ was detected as the soluble phase and the insoluble phases were $ZnFe_2O_4$ and $ZnSiO_3$ respectively. In BOF OG, three zinc species were identified, that is $Zn_5(CO_3)_2(OH)_6$, $ZnFe_2O_4$ and $ZnSO_4 \cdot 7H_2O$. Extended X-ray absorption fine structure (EXAFS) data analysis indicated the presence of Zn–O, Zn–Fe, Zn–Zn bonds in the nearest two coordination shells in EAFD and BOF LT identifying the significant content of franklinite. In BOF OG, only Zn–O and Zn–Zn bonds occurred in the nearest two coordination shells. On the basis of the above results, possible methods for improving the recycling methods of each type of zinc-containing steelmaking wastes were discussed. Obviously, these results not only provide us with fundamental information about the zinc speciation at the molecular scale in dust and sludge but also demonstrated the essential importance of the characterization of zinc speciation for developing recycling strategies.

Acknowledgements

This work was supported by the project of Chinese Academy of Science (no. KJCX2-YW-N43) and National Nature Science Foundation of China (Grant no. 11105208). BL14B beamline at Shanghai Synchrotron Radiation Facility is also appreciated for providing the beamline time to do SR-based XRD experiments.

References

1 J. Vymazal, *Acta Hydrochim. Hydrobiol.*, 1985, **13**, 627–635.
2 I. Y. R. Adamson, H. Prieditis, C. Hedgecock and R. Vincent, *Toxicol. Appl. Pharmacol.*, 2000, **166**, 111–119.
3 I. E. Doronin and A. G. Svyazhin, *Metallurgist*, 2011, **54**(9–10), 673–681.
4 Z. Li, *Baosteel Technol.*, 2002, **6**, 18–20.
5 R. A. Shawabkeh, *Hydrometallurgy*, 2010, **104**, 61–65.
6 P. Oustadakis, P. E. Tsakiridis, A. Katsiapi and S. Agatzini-Leonardou, *J. Hazard. Mater.*, 2010, **179**, 1–7.
7 T. Havlík, B. V. Souza, A. M. Bernardes, I. A. H. Schneider and A. Miškufová, *J. Hazard. Mater. B*, 2006, **135**, 311–318.
8 A. J. B. Dutra, P. R. P. Paiva and L. M. Tavares, *Miner. Eng.*, 2006, **19**, 478–485.
9 N. Leclerc, E. Meux and J.-M. Lecuire, *J. Hazard. Mater.*, 2002, **91**, 257–270.
10 R. P. W. J. Struis, C. Ludwig, H. Lutz and A. M. Scheidegger, *Environ. Sci. Technol.*, 2004, **38**, 3760–3767.
11 C. Samuelsson and G. Carlsson, *CIM Bull.*, 2001, **94**(1051), 111–115.
12 A. C. Scheinost, R. Kretzschmar and S. Pfister, *Environ. Sci. Technol.*, 2002, **36**, 5021–5028.
13 A. Manceau, B. Lanson, M. L. Schlegel, J. C. Hargé, M. Musso, L. Eybert-Bérard and G. M. Lamble, *Am. J. Sci.*, 2000, **300**, 289–343.
14 M. Nachtegaal, M. A. Marcus, J. E. Sonke, J. Vangronsveld, K. J. T. Livi, D. van. Der Lelle and D. L. Sparks, *Geochim. Cosmochim. Acta*, 2005, **69**(19), 4649–4664.
15 M.-P. Isaure, A. Laboudigue, A. Manceau, G. Sarret, C. Tiffreau, P. Trocellier, G. Lamble, J.-L. Hazemann and D. Chateigner, *Geochim. Cosmochim. Acta*, 2002, **66**(9), 1549–1567.
16 S. Endo, Y. Terada, Y. Kato and I. Nakai, *Environ. Sci. Technol.*, 2008, **42**, 7152–7158.
17 J. Kawai, in *Developments in Soil Science 34: Synchrotron-based Techniques in Soils and Sediments*, ed. B. Singh and M. Grafe, Elsevier, Burlington, MA, 2010, pp. 131–146.
18 M. Takaoka, T. Yamamoto, A. Shiono, N. Takeda, K. Oshita, T. Matsumoto and T. Tanaka, *Chemosphere*, 2005, **59**, 1497–1505.
19 M. L. Sammut, Y. Noack, J. Rose, J. L. Hazemann, O. Prous, M. Depoux, A. Ziebel and E. Fiant, *Chemosphere*, 2010, **78**, 445–450.
20 J. Kawai, S. Hayakawa, F. Esaka, S. Zheng, Y. Kitajima, K. Maeda, H. Adachi, Y. Gohshi and K. Furuya, *Anal. Chem.*, 1995, **67**, 1526–1529.
21 M. G. Tan, G. L. Zhang, X. L. Li, Y. X. Zhang, W. S. Yue, J. M. Chen, Y. S. Wang, A. G. Li, Y. Li, Y. M. Zhang and Z. C. Shan, *Anal. Chem.*, 2006, **78**, 8044–8050.
22 A. L. Foster, G. E. Brown Jr., T. N. Tingle and G. A. Parks, *Am. Mineral.*, 1998, **83**, 553–568.
23 A. J. Slowey, J. J. Rytuba and G. E. Brown, Jr, *Environ. Sci. Technol.*, 2005, **39**, 1547–1554.
24 A. Bernaus, X. Gaona, J. M. Eabrí, P. Higueras, G. Falkenberg and M. Valiente, *Environ. Sci. Technol.*, 2006, **40**, 4090–4095.
25 B. Ravel and M. Newville, *J. Synchrotron Rad.*, 2005, **12**, 537–541.
26 Bruce Ravel, ATHENA Use's Guide, http://cars9.uchicago.edu/~ravel/software/exafs/.
27 http://cars9.uchicago.edu/atomsdb/ZnFe2O4.inp.
28 S. Ghose, *Acta Cryst.*, 1964, **17**, 1051–1057.
29 C. L. Li and M. S. Tsai, *J. Mater. Sci.*, 1993, **28**, 4562–4570.
30 J. G. M. S. Machado, F. A. Brehm, C. A. M. Moraes, C. A. dos Santo, A. C. F. Vilela and J. B. M. da Cunha, *J. Hazard. Mater. B*, 2006, **136**, 953–960.

31 B. Linblom, C. Samuelsson, Å. Sandström and G. Ye, *JOM*, 2002, **54**(12), 35–38.
32 S. J. Stewart, S. J. A. Figueroa, J. M. R. López, S. G. Marchetti, J. F. Bengoa, R. J. Prado and F. G. Requejo, *Phys. Rev. B: Condens. Matter Mater. Phys.*, 2007, **75**, 073408.
33 S. J. A. Figueroa and S. J. Stewart, *J. Synchrotron Rad.*, 2009, **16**, 63–68.
34 C. E. R. Torres, F. Golmar, M. Ziese, P. Esquinazi and S. P. Heluani, *Phys. Rev. B: Condens. Matter Mater. Phys.*, 2011, **84**, 064404.
35 M. Yu, S. Tian, W. Chu, D. Chen, Q. Wang and Z. Wu, *J. Synchrotron Radiat.*, 2009, **16**, 528–532.
36 M. L. Sammut, Y. Noack and J. Rose, *J. Geochem. Explor.*, 2006, **88**, 239–242.
37 D. R. Roberts, A. C. Scheinost and D. L. Sparks, *Environ. Sci. Technol.*, 2002, **36**, 1742–1750.
38 C. Xu, R. Lin and D. Wang, *Physical Chemistry of Zinc Metallurgy*, 1997, pp. 64–66.
39 R. G. Ford and D. L. Sparks, *Environ. Sci. Technol.*, 2000, **34**, 2479–2483.
40 A. Manceau, M. L. Schlegel, M. Musso, V. A. Sole, C. Gauthier, P. E. Petit and F. Trolard, *Geochim. Cosmochim. Acta*, 2000, **64**, 3643–3661.
41 T. P. Trainor, G. E. Brown, Jr and G. A. Parks, *J. Colloid Interface Sci.*, 2000, **231**, 359–372.
42 J. Ha, T. P. Trainor, F. Farges and G. E. Brown, Jr, *Langmuir*, 2009, **25**(10), 5574–5585.
43 R. G. Ford and D. L. Sparks, *Environ. Sci. Technol.*, 2000, **34**, 2479–2483.
44 L. Shi, R. Chen and R. Wang, *Chinese Resources Comprehensive Utilization*, 2008, vol. 26(2), pp. 12–15.
45 L. Shi, R. Chen and R. Wang, *Chinese Resources Comprehensive Utilization*, 2009, vol. 27(2), pp. 19–22.
46 R. A. Shawabken, *Hydrometallurgy*, 2010, **104**, 61–65.
47 N. Leclerc, E. Meux and J.-M. Lecuire, *Hydrometallurgy*, 2003, **70**, 175–183.
48 Z. Youcai and R. Stanforth, *J. Hazard. Mater. B*, 2000, **80**, 223–240.
49 M. K. Jha, V. Kumar and R. J. Singh, *Resour., Conserv. Recycl.*, 2001, **33**, 1–22.
50 Y. Zhao and R. Stanforth, *Miner. Eng.*, 2000, **13**(13), 1417–1421.
51 J. A. Stegemann, A. Roy, R. J. Caldwell, P. J. Schilling and R. Tittsworth, *J. Environ. Eng.*, 2000, 112–120.